

# On-chip cavity quantum phonodynamics with an acceptor qubit in silicon

Rusko Ruskov and Charles Tahan

Laboratory for Physical Sciences, 8050 Greenmead Dr., College Park, MD 20740\*

We describe a chip-based, solid-state analogue of cavity-QED utilizing acoustic phonons instead of photons. We show how long-lived and tunable acceptor impurity states in silicon nanomechanical cavities can play the role of a matter non-linearity for coherent phonons just as, e.g., the Josephson qubit plays in circuit-QED. Both strong coupling (number of Rabi oscillations  $\lesssim 100$ ) and strong dispersive coupling (0.1-2 MHz) regimes can be reached in cavities in the 1-20 GHz range, enabling the control of single phonons, phonon-phonon interactions, dispersive phonon readout of the acceptor qubit, and compatibility with other optomechanical components such as phonon-photon translators. We predict explicit experimental signatures of the acceptor-cavity system.

Circuit-QED has revolutionized the field of cavity-QED (cQED) [1–3] providing a stable platform for light-matter interaction in the microwave regime along with large couplings and solid state integrability. Progress in the field has enabled applications such as single microwave photon sources [4] and quantum logic gates [3] on a chip. In an ideal crystal environment, phonons may play a role analogous to photons, though they propagate with the much slower speed of sound. That acoustic phonons can be quantum coherent has been explored in a number of architectures, allowing seminal experiments in optomechanical cooling [5–10], trapping of phonons in phononic bandgap cavities [6, 10], photon translation via phonons [11], and indirect qubit-phonon coupling [12, 13]. What is missing to complete the analogy for phonons is a non-linear element similar to an atom in cQED.

Such an element is possible, where an impurity transition in a crystal (e.g., two-levels of a Si donor) couples *directly* to confined phonons to form a hybridized state, which has been referred to as a phoniton (in analogy with a polariton) [14]. The impurity-phonon interaction can be large due to a large deformation potential:  $\langle \psi_s | \hat{D}_{ij} | \psi_s \rangle \sim \text{eV}$  [15]. The previously proposed system utilizing an Umklapp *valley* transition [14, 16] of a donor in Si, however, requires very high frequencies (a few hundred GHz) and can be difficult to integrate with other phonon components. While other impurities such as in diamond [13] or in III-V semiconductors can offer smaller frequencies, a practical system in silicon would be highly desirable given recent demonstrations of high-Q cavities in silicon nanostructures [10, 17], silicon's investment in materials quality, and compatibility with CMOS technology and silicon photonics.

Here we propose a new quantum circuit element based on a single acceptor (such as B, Al, In) embedded in a patterned silicon nano-membrane, and driven by a long wavelength phonon,  $\lambda_{\text{phon}} \gg a_{\text{acceptor}}^* \sim \text{few nm}$ , compatible with opto/mechanical components [6, 10]. The acceptor two-level system (qubit), Fig. 1, has already been proposed for quantum computing [18] and is easily tunable in the 1 – 50 GHz range by external magnetic field and also by electric field or strain (allowing multiple qubit choices). We show how the acceptor-cavity system allows for both strong resonant coupling (where the qubit-phonon coupling,  $g$ , is greater than the loss mechanisms of the qubit and cavity,  $\Gamma_{\text{qb}}, \kappa_{\text{cav}}$ , respec-

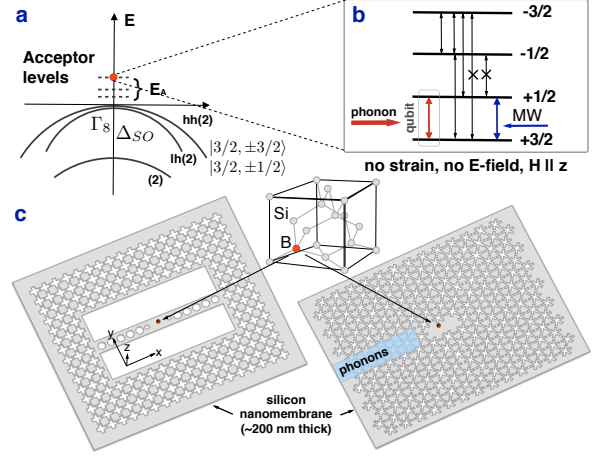


FIG. 1. Acceptor:Si nanomechanical-cavity-phoniton. (a) Hole valence bands in Si; 4-fold degeneracy at the band top (and of lowest acceptor states) corresponds to particles of spin  $J = 3/2$  ( $\Gamma_8$  representation of cubic symmetry, see, e.g. Ref.[15]). (b) Ground state splitting via external magnetic field along  $[0,0,1]$  direction; allowed (forbidden) phonon transitions and qubit phonon driving (see text). Level rearrangement is via additional strain. System manipulation via electric static/microwave fields is possible. (c) Nanomechanical 1D and 2D phonon bandgap cavities reminiscent of already fabricated high-Q cavities in a patterned Si membrane [6, 10]; an on-chip phonon waveguide allows coupling to the phoniton system.

tively) and strong dispersive coupling, enabling the observability of a phonon vacuum Rabi splitting, and QND measurement of the cavity phonon number. Experimental signatures of the system are given, via magnetic field and temperature dependence (for  $T \lesssim 1\text{K}$ ), utilizing optical techniques.

*Engineering the qubit levels.* Two acceptor qubit arrangements are possible based on the lifting of the 4-fold ground state degeneracy via external fields [19]. For a magnetic field  $\mathbf{H}_z = (0,0,H_z)$  along the crystal  $[0,0,1]$  growth direction one can choose the lowest two Zeeman levels,  $|\phi_1\rangle = |3/2\rangle$ ,  $|\phi_2\rangle = |1/2\rangle$ , as the qubit, which is the primary focus of this paper (Fig. 1b). The Zeeman type interaction is given by [15, 20]:  $H_H = \mu_B \{ g'_1 \mathbf{J} \mathbf{H} + g'_2 (J_x^3 H_x + \text{c.p.}) \}$ ; here c.p. is cyclic permutation of  $x,y,z$ ;  $J_x, \dots$ , etc. are the spin  $3/2$  matrices (in the crystal directions), and the renormalized  $g$ -values  $g'_1, g'_2$  ( $\mu_B$  is Bohr magneton), depending on the ac-

ceptor bound states, fulfill the relations  $|g'_1| \approx 1$ ,  $|g'_2| \ll |g'_1|$  [15, 21, 22]. The qubit splitting  $\delta E_H \simeq \mu_0 g'_1 H$  is tunable in the range  $\approx 1 - 40$  GHz for  $H = 0.1 - 3$  T. The term  $\sim g'_2 J_x^3$  lifts the equidistancy: the outer splittings (Fig. 1b) are larger than the middle one by  $\frac{3g'_2}{g'_1} \simeq 0.09$ . For a field  $\mathbf{H}$  tilted away from the crystal axis the qubit splitting is weakly angle dependent.

Alternatively, a second qubit arrangement involves mechanical stress in addition to the magnetic field. Stress lifts the ground state degeneracy only partially: e.g., for stress along the crystal  $\hat{z}$ -direction (Fig. 1c), states  $|\pm 3/2\rangle$  and  $|\pm 1/2\rangle$  remain degenerate. Providing the stress causes a splitting larger than the magnetic field splitting, the levels in Fig. 1b rearrange so that the lowest (qubit) levels will be  $|\phi'_1\rangle = |-1/2\rangle$ ,  $|\phi'_2\rangle = |1/2\rangle$ . This forms an alternate “phonon protected” qubit, decoupled from phonons to first order (the coupling can be switched on via electric field, see below). The effect of strain,  $\epsilon_{\alpha\beta}$ , is described by the Bir-Pikus Hamiltonian[15]:

$$H_E = a' \text{Tr} \epsilon_{\alpha\beta} + b' \epsilon_{xx} J_x^2 + \frac{d'}{\sqrt{3}} \epsilon_{xy} \{J_x J_y\}_+ + \text{c.p.} \quad (1)$$

Experimentally [21] the deformation potentials for B:Si are:  $b' \simeq -1.42$  eV,  $d' \simeq -3.7$  eV. We estimate a splitting of  $\delta E_E \approx 1 - 10$  GHz for external stress of  $10^5 - 10^6$  Pa [23]. A larger stress would suppress the qubit-phonon coupling.

*Strong coupling of acceptor to confined acoustic phonon.* Here, we focus on the qubit  $\{1 = |3/2\rangle, 2 = |1/2\rangle\}$  that does not require static strain. The coupling to a phonon mode is calculated by adding a quantized phonon field [19] in addition to any classical field. We consider coupling to a plane wave  $\epsilon_{\text{vac}} \xi_q^{(\sigma)} e^{-i\mathbf{q}\cdot\mathbf{r}}$  with polarization  $\xi_q^{(\sigma)}$  (transverse,  $t_1, t_2$ , or longitudinal,  $l$ ) and energy  $\hbar v_{\sigma} q$ , that proved to be a good estimation of coupling to modes with realistic boundaries [14]. Moreover, the acceptor transition, unlike the {P/Li}:Si valley transition [14, 16], is less sensitive to the details of the confined phonon mode since the dipole approximation applies. The matrix element is proportional to the “phonon vacuum field”,  $\epsilon_{\text{vac}} \equiv \left(\frac{\hbar q}{2\rho v_{\sigma}}\right)^{1/2}$ ;  $\rho$ ,  $\mathcal{V}$ , and  $v_{\sigma}$  are the mass density, mode volume, and sound velocity in Si. The coupling is (acceptor is placed at maximum *strain* unlike in [14] where the valley transition requires placing at maximum *displacement*):

$$g_{\sigma}^{3/2,1/2} = d' \left( \frac{\hbar \omega_{12}}{8\rho \hbar^2 v_{\sigma}^2} \right)^{1/2} \begin{Bmatrix} \cos \theta, \sigma = t_1 \\ i \cos 2\theta, \sigma = t_2 \\ -i \sin 2\theta, \sigma = l \end{Bmatrix} e^{-i\varphi}, \quad (2)$$

where the polar angles,  $\theta, \varphi$  of the wave vector  $\mathbf{q}$  are with respect to  $\mathbf{H} \parallel \hat{z}$ . Thus, the mode  $t_2$  has a maximum along the phonon cavity ( $\theta \approx \pi/2$ ), Fig. 1c. An alternative is to have an in-plane magnetic field  $\mathbf{H}_x$  along the crystal  $[1, 0, 0]$   $\hat{x}$ -direction (the latter is chosen to be along the cavity): both modes  $t_1, t_2$  (now at  $\theta \approx 0$ ) are preferably coupled to the cavity. The maximal coupling  $g_{\text{max}, \sigma}^{3/2,1/2}$  scales as  $\propto \sqrt{q/\mathcal{V}}$ , as expected for a ( $1s \rightarrow 1s$ ) transition. For a cavity volume  $\mathcal{V} \simeq d\lambda^2$  ( $d = 200$  nm is the Si membrane thickness) we get coupling in the range  $g/2\pi \simeq 0.4 - 21$  MHz for  $1 - 14$  GHz (Table 1). The

other allowed transition  $|3/2\rangle \rightarrow |-1/2\rangle$  (at twice the qubit frequency) is well detuned; the transitions  $|3/2\rangle \rightarrow |-3/2\rangle$ ,  $|1/2\rangle \rightarrow |-1/2\rangle$  are phonon forbidden (Fig. 1b).

Generally, when the in-plane magnetic field has some angle  $\theta_0$  with the cavity (crystal  $x$ -axis), all transitions are allowed. Also, the qubit coupling to a preferably confined cavity phonon will change. As a qualitative example, consider a plane wave transverse mode  $t_1$  (or  $t_2$ ) along the  $x$ -axis ( $\theta \approx 0$ ): the coupling will change in the same way as in Eq. (2), with  $\theta$  replaced by  $\theta_0$ . This allows manipulation of the qubit-cavity coupling by rotation of the magnetic field.

*Qubit relaxation rate.* The qubit relaxation in the cavity is bounded at low temperatures by the bulk phonon spontaneous emission rate, we find:

$$\Gamma_{3/2,1/2}(\theta_0) = \frac{(\hbar \omega_{12})^3}{20\pi \rho \hbar^4} \left\{ d'^2 (\cos^2 2\theta_0 + 1) \left[ 2/3 v_l^5 + 1/v_t^5 \right] + b'^2 \sin^2 2\theta_0 \left[ 2/v_l^5 + 3/v_t^5 \right] \right\}; \quad (3)$$

here  $l$ -phonon contribution is a small percent. The results in Table 1 are for  $\theta_0 = 0$ . Note that the coupling in this case can be switched off (e.g. for a  $t_1$ -mode along  $\hat{x}$ -direction, at  $\theta_0 = \pi/2$ ) while the relaxation cannot.

For the alternate qubit,  $\{|-1/2\rangle, |1/2\rangle\}$ , the stress and magnetic field are parallel along the  $\hat{z}$ -direction (Fig. 1c). Here both coupling and relaxation are zero in the absence of electric field and can be switched on using non-zero electric field  $\mathbf{E}_z$  in the same direction [19]. The qubit-phonon coupling is given by the same Eq.(2) multiplied by a coupling factor, a function of the splitting ratios  $r_h \equiv \frac{\delta E_H}{\delta E_E}$ ,  $r_e \equiv \frac{\delta E_E}{\delta E_e}$ :  $f(r_h, r_e) = (\sqrt{z_+ z_-} - 1) / \sqrt{(1+z_+)(1+z_-)}$ , with  $z_{\pm} = (1 \pm \sqrt{(1 \mp r_h)^2 + r_e^2 \mp r_h^2}) / r_e^2$ . Thus, e.g. for  $r_h = 0.5 - 0.9$  this factor reaches  $\approx 0.25 - 0.65$  for some optimal value of the electric field splitting,  $r_e \lesssim 1$ , which allows strong coupling.

The calculated relaxation times from Eq.(3) (Table 1) are comparable to that in bulk Si [27] at low B:Si doping ( $8 \times 10^{12} \text{ cm}^{-3}$  or 500 nm acceptor spacing), where  $T_1^{\text{echo}} \simeq 7.4 \mu\text{s}$  and  $T_2^{\text{echo}} \simeq 2.6 \mu\text{s}$  were measured at 45 mK. Note that the single acceptor linewidth ( $\sim 1/T_{2,\text{single}}^*$ ) is the proper metric to compare  $g$  with, not the inhomogeneously broadened  $1/T_2^*$  obtained from ensemble measurements [28]. While  $T_2 = 2T_1$  for phonons alone, it may be limited by electric-dipole coupling to impurities [18], magnetic hyperfine coupling to nearby nuclei  $^{29}\text{Si}$  (expected to be small for holes), or charge noise (though here the acceptor is far away from surfaces or metal gates); both  $T_1, T_2$  may improve for defect-free, low-doped, [21, 22, 29] and isotopically purified samples [28, 30];  $T_1$  may also improve in nanomembranes ( $d \ll \lambda$ ) due to phase-space suppression (less available modes).

*Phonon cavity loss.* In the 1D/2D-phononic bandgap Si nanomembranes considered here (Fig. 1c), the main cavity loss mechanism is due to (fabrication) symmetry-breaking effects, coupling the cavity mode to unconfined modes, and also due to cavity surface defects [17]. Bulk losses are negligible in the few GHz range [14, 17]. In this range the cavity  $Q$ -factor,  $Q \equiv \kappa/\omega$ , can reach  $10^4 - 10^5$ , or higher [10, 17].

parameter	symbol	circuit-QED	Quant Dot-QED	B:Si (1 GHz)	B:Si (4 GHz)	B:Si (8 GHz)	B:Si (1 Tesla)
resonance freq.	$\omega_r/2\pi$	5.7 GHz	325 THz	1 GHz	4 GHz	8 GHz	14 GHz
vac. Rabi freq.	$g/2\pi$	105 MHz	13.4 GHz	0.41 MHz	3.27 MHz	9.26 MHz	21.4 MHz
cavity lifetime	$1/\kappa, Q$	$0.64 \mu\text{s}, 10^4$	$5.5 \text{ ps}, 1.2 \cdot 10^4$	$15.9 \mu\text{s}, 10^5$	$4 \mu\text{s}$	$2 \mu\text{s}$	$1.14 \mu\text{s}$
qubit lifetime	$1/\Gamma$	84 ns	27 ps	$386.5 \mu\text{s}$	$6 \mu\text{s}$	$0.75 \mu\text{s}$	$0.14 \mu\text{s}$
critical atom #	$2\Gamma\kappa/g^2$	$\lesssim 8.6 \cdot 10^{-5}$	$\lesssim 1.87$	$\lesssim 4.9 \cdot 10^{-5}$	$\lesssim 2 \cdot 10^{-4}$	$\lesssim 3.9 \cdot 10^{-4}$	$\lesssim 6.9 \cdot 10^{-4}$
crit. phonon #	$\Gamma^2/2g^2$	$\lesssim 1.6 \cdot 10^{-4}$	$\lesssim 9.4 \cdot 10^{-2}$	$\lesssim 5.1 \cdot 10^{-7}$	$\lesssim 3.2 \cdot 10^{-5}$	$\lesssim 2.6 \cdot 10^{-4}$	$\lesssim 1.4 \cdot 10^{-3}$
# Rabi flops	$2g/(\kappa+\Gamma)$	$\sim 98$	$\sim 0.8$	$\sim 79$	$\sim 99$	$\sim 64$	$\sim 34$
cavity volume	$\mathcal{V}$	$10^{-6} \lambda^3$	-	$0.037 \lambda^3$	$0.148 \lambda^3$	$0.296 \lambda^3$	$0.52 \lambda^3$
wavelength	$\lambda$	5.26 cm	921 nm	5400 nm	1350 nm	675 nm	385 nm
dispersive coupling	$\chi \equiv g^2/\Delta$	17 MHz	-	0.04 MHz	0.33 MHz	0.93 MHz	2.14 MHz
peaks' resolution	$2\chi/\Gamma$	$\sim 6$	-	$\sim 199$	$\sim 25$	$\sim 9$	$\sim 4$
# of peaks	$2\chi/\kappa$	$\sim 70$	-	$\sim 8$	$\sim 16$	$\sim 23$	$\sim 31$

TABLE I. Key parameters for circuit-QED [25] (1D cavity), Quantum dot(QD)-QED [26] vs. the  $\{|3/2\rangle, |1/2\rangle\}$  B:Si phoniton in a patterned Si membrane (of thickness  $d = 200 \text{ nm}$ ) phononic bandgap cavity; we show calculations for maximal coupling at frequencies of 1 GHz, 4 GHz, 8 GHz, and 14 GHz, for cavity volume  $\mathcal{V} = d\lambda^2$  and  $Q = 10^5$ , using bulk  $T_1$ -limited linewidth  $\Gamma$ . The limiting frequency for strong dispersive coupling is reached at  $\approx 21 \text{ GHz}$ , when  $\chi = \Gamma$ ; dressed state's resolution parameters are comparable to that in circuit-QED.

Calculated rates in Table 1 show that *strong resonant coupling* is possible:  $g_{12} \gg \Gamma_{12}, \kappa$  in a wide frequency range, allowing  $\sim 30 - 100$  Rabi flops. The low limit of 1 GHz is for  $T \simeq 20 \text{ mK}$ , unless an active cavity cooling is performed [10]; a high limit of  $\sim 200 \text{ GHz}$  is set by the different energy scaling of  $g$  and  $\Gamma$ . At high frequencies the  $Q$ -factor will decrease; still, e.g., at 14 GHz even  $Q = 10^3$  leads to strong coupling.

*Observing the vacuum Rabi splitting.* A suitable observable is the averaged phonon cavity field amplitude  $|\langle \hat{b} \rangle|$ , which we have calculated, Fig. 2a-d, taking into account the first two excited dressed states (a “two-state approximation”, [32]). On Fig. 2a we show the  $\langle \hat{b} \rangle$ -spectrum ( $\omega_r$  is the cavity frequency) for  $\omega_a = \omega_r = 8 \text{ GHz}$  as two Rabi peaks at  $\pm g$  vs. external phonon driving frequency  $\omega_d$ , while Fig. 2c shows the “anti-crossing picture” of the spectra at different acceptor detuning  $\Delta_{ar} = \omega_a - \omega_r$ . Here the left resonance width and height are  $\Gamma_L = \sin^2 \Theta_0 \Gamma + \cos^2 \Theta_0 \kappa$  and  $\cos \Theta_0$ , and for the right resonance one replaces  $\sin \Theta_0 \leftrightarrow \cos \Theta_0$ , with  $\tan(2\Theta_0) = 2g/\Delta_{ar}$ .

Another option to observe the dressed resonance(s) is to sweep the qubit detuning (via the  $H$ -field) while keeping the input in resonance with the phonon cavity. As seen from Fig. 2c, the field amplitude will exhibit a resonant dip, shown for different cavity frequencies, Fig. 2d. For large detuning the resonance is approximately a Lorentzian with a full width at half maximum,  $\{\text{fwhm}\} \approx g^2/\kappa$  (a weak dependence on the qubit relaxation  $\Gamma$  is suppressed for strong coupling).

With increasing temperature the Rabi peak will be broadened [33] by the factor  $1 + 2n_{\text{th}}$  and the peak height will decrease by  $2p_{\text{st}} - 1$ , where  $p_{\text{st}} = (1 + n_{\text{th}})/(1 + 2n_{\text{th}})$  is the ground state occupation. This is relevant for small thermal phonon number,  $n_{\text{th}} \equiv 1/(\exp[\hbar\omega_r/k_B T] - 1)$ , at low  $T$  ( $n_{\text{th}} \lesssim 0.2$ ; see, e.g., Ref. [34]). For  $\omega_r/2\pi = 8 \text{ GHz}$  the Rabi peaks will be seen at 350 mK, but are negligible at 1 K (Fig. 2b). At higher  $T$ , when  $n_{\text{th}} \gtrsim 1$ , the lowest dressed states become saturated and in addition two broadened peaks will appear (inside the Rabi doublet, Fig. 2a), at  $\delta\omega_d \simeq \pm g[\sqrt{n+1} - \sqrt{n}]$ ,  $n \approx n_{\text{th}}$ . These will dominate over the Rabi peaks [34], providing a signature of strong coupling even beyond 1 K.

*Measurement via photons and standard techniques.* Ideally,

one would probe the acceptor-cavity system with phonons. Direct phonon creation and detection should be possible via acoustic transducers [35]. As in circuit QED [36], phonon correlations can be measured even without single phonon counters. However, here we consider an approach with single phonon sensitivity using a phonon-to-photon translator (PPT) [31] that can be realized on the same nanomembrane (with a photon/phonon bandgap, see Figs. 1c, 2e).

The PPT allows for optical techniques [7, 10] to be applied to phononics. We show in Fig. 2e an experimental schematic, to measure the phonon cavity field  $\langle \hat{b} \rangle$  via a homodyne/heterodyne optical measurement [33]. To scan around the mechanical resonance  $\omega_r$ , one needs optical frequency resolution (at  $\omega/2\pi \approx 200 \text{ THz}$ ) better than the dressed state width,  $(\Gamma + \kappa)/2\pi \approx 30 - 150 \text{ kHz}$ , Table 1. In the on-chip PPT implementation no photon should enter the phoniton system, to avoid acceptor ionization. However, the estimated ionization cross section is small,  $\sigma_{\text{phot}} \approx 8.6 \times 10^{-23} \text{ m}^2$ : for 10 photons in the cavity, at maximum photon-acceptor overlap, one gets an ionization lifetime of  $12 \mu\text{s}$ , that can be further increased in regions of low photon intensity [19].

A strong *dispersive coupling*,  $\chi \equiv g^2/\Delta_{ar}$ , is reachable as per Table 1. Since  $\Delta_{ar} \geq 10g$  (dispersive regime) and  $g^2/\Delta_{ar}\Gamma_{\text{relax}} \geq 1$  (good resolution of phonon numbers), resolving the number states  $|n\rangle$  in the phononic cavity would be possible. In the dispersive regime one can apply two tones (as in circuit-QED [25]): here, one tone is a *phonon* probe at  $\omega_d$ , slightly detuned from the resonator (Fig. 2e). The second (spectroscopic) tone, at  $\omega_{sp}$ , is driving some of the dressed transitions around the acceptor frequency, at  $\omega_a + (2n+1)\chi$ , via electric microwaves (MW), similar to a manipulation of individual nitrogen-vacancy centers [13] (for B:Si a stronger MW coupling [22, 27] is expected compared to NVc). Thus, one could observe the *fine spectral structure* of the dressed cavity-acceptor system, predicted by Ref. [37] in a different context, by measuring the phonon (photon) reflection while sweeping the MW tone  $\omega_{sp}$ . We note that other measurement approaches are possible via, e.g., hole transport [24, 38] or STM probe spectroscopy [39].

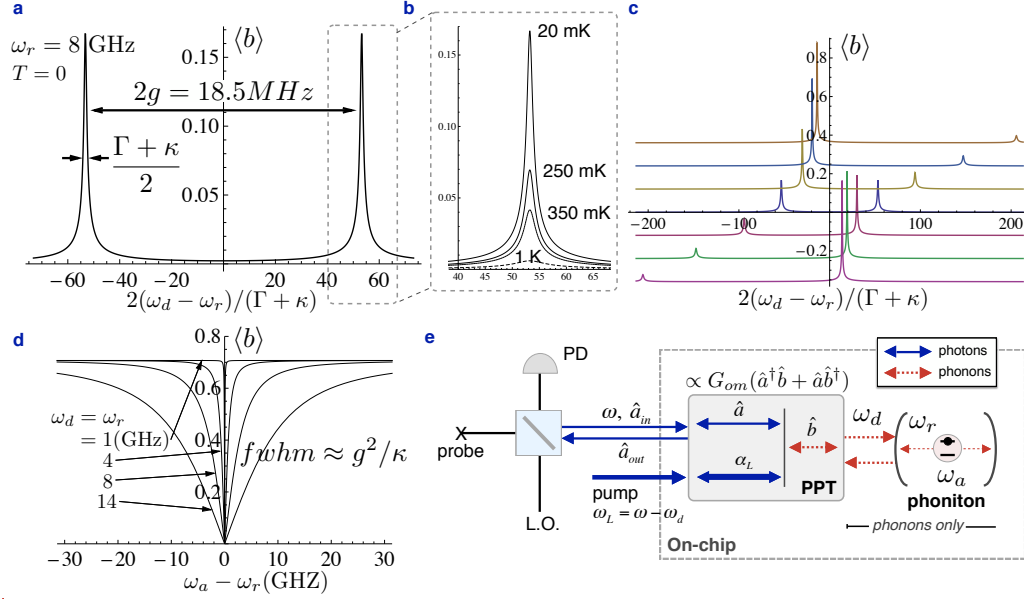


FIG. 2. Intracavity field  $\langle \hat{b} \rangle$  vs. frequencies and temperature. (a) Rabi splitting in the strong resonant coupling regime as a function of a phonon signal sweep. (b) Rabi peaks vs. temperature (approximate). At  $n_{th} \gtrsim 1$  broad peaks will appear inside the Rabi doublet (not shown) due to transitions to higher dressed states (see text). (c) “Anticrossing picture” at qubit-phonon cavity detuning,  $\Delta_{ar}$  (curves vertically shifted for clarity); for large positive detuning (upmost curve), the left resonance is dispersively shifted by  $-g^2/\Delta_{ar}$  while the right resonance is suppressed as  $\sin \Theta_0$  (see text). (d) An alternative to determine the Rabi splitting: the absorption spectrum as a function of qubit detuning (via a magnetic field sweep). (e) Schematics of an optical homodyne/heterodyne experiment (see also Ref. [7]) utilizing a PPT [19, 31].

*Discussion and applications.* We have introduced a system that allows for on-chip manipulation of coherent acoustic phonons via coupling to acceptor qubit states in a nanomechanical cavity. Hybridization of the phonon-acceptor system and strong dispersive coupling are possible with comparable parameters to circuit-QED [25] and far surpassing semiconductor QD QED [26]. The cavity-phonon can be incorporated in more complex networks such as with phonon-photon interfaces to photonics [10, 31], and in arrays of phonitons for engineered many-body phonon devices [14, 40]. From the perspective of qubits [18, 41], the isolated acceptor provides a potentially robust two-level system for quantum information processing. Our system offers an avenue for phonon dispersive readout of acceptor qubits and the potential for spin qubit-to-photon conversion in silicon.

## SUPPLEMENTAL MATERIAL

*Hole valence bands in Si.* Holes in Si require a richer physical picture [15, 20] (compared to positrons in QED). The 4-fold degeneracy (Fig. 1a, main text) at the top of the valence band (neglecting heavy-light hole splitting) corresponds to propagation of particles of spin  $J = 3/2$ , reflecting the  $\Gamma_8$  representation of cubic symmetry. Relatively large spin-orbit coupling implies a 2-fold degenerate band ( $\Gamma_7$  representation), split-off by an energy gap  $\Delta_{SO} \simeq 45$  meV [15]. The role of an “atom” can be taken by a single impurity in a host crystal, e.g. in Si. For shallow acceptor centers in Si (e.g., B, Al, In, etc)

the ionization energy is  $E_A \sim \Delta_{SO}$ : thus, all valence bands will play a role in the acceptor states. Still, the lowest acceptor states remain 4-fold degenerate since the acceptor spherical (Coulomb) potential does not change the cubic symmetry of the host crystal [15].

*Origin of strong acceptor-phonon coupling.* The impurity-acoustic phonon interaction [15],  $H_{e,ph}^{ac}(\mathbf{r}) = \sum_{ij} \hat{D}_{ij} \hat{\epsilon}_{ij}(\mathbf{r})$ , may lead to a strong coupling regime ( $g > \Gamma_{qb}, \kappa_{cav}$ ) even for cavity effective volume of few tens [14] of  $\sim \lambda^3$ , since the deformation potential matrix elements are large [15]:  $\langle \psi_s | \hat{D}_{ij} | \psi_s \rangle \sim \text{eV}$ . Qualitatively, the large coupling can be traced from the much smaller bandgap ( $\sim \text{eV}$ ) in the “Si-vacuum” as compared to QED ( $\sim 10^6 \text{eV}$ ). For the spin transitions of interest (e.g.,  $3/2 \rightarrow 1/2$ ) the spin states are actually “compound” states of  $P$ -like Bloch orbitals (spin 1) and electronic spin-1/2. Thus, coupling via deformation (a phonon) of the crystal is possible due to different orbital content of these states.

*Engineering the qubit levels.* *The role of electric field.* The degeneracy of the ground state can be lifted by external magnetic field via the Zeeman type interaction  $H_H$  (Fig. 3a), and via mechanical strain (Fig. 3b) (see Eq. (1) of main text). The related Hamiltonians are invariants of the cubic symmetry group  $O_h = T_d \times I$  and time reversal [15, 20] and are constructed from the momentum operator,  $k_\alpha = \frac{1}{i} \frac{\partial}{\partial x_\alpha} + \frac{e}{c} A_\alpha$  (or the corresponding fields [15]) and the spin-3/2 operators  $J_\alpha$ ,  $\alpha = x, y, z$ .

For a relatively weak electric field  $\mathbf{E}$  the linear Stark effect

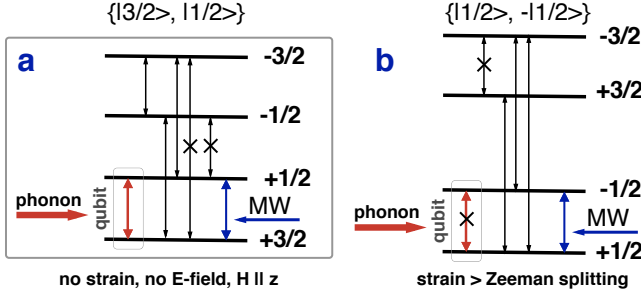


FIG. 3. Two possible level arrangements as described in main text. (a) Splitting due to magnetic field along a crystal direction (e.g.  $\hat{H}||\hat{z}$ ). Equidistance is lifted by the cubic term, leading the 9% smaller (for  $g_1g_2 < 0$ ) splitting of the levels  $-1/2, 1/2$ . The qubit,  $\{|1/2\rangle, |3/2\rangle\}$ , is coupled strongly to a confined phonon, and can be manipulated via MWs. (b) Level splitting in presence of magnetic field and stress along the  $\hat{z}$ -direction, in the case of  $\delta E_e > \delta E_H$ . The alternate qubit,  $\{|-1/2\rangle, |1/2\rangle\}$ , is decoupled from phonons (to first order). The coupling can be switched on via suitable electric field in the same direction.

is possible:

$$H_E = \frac{pE}{\sqrt{3}} (E_x\{J_yJ_z\}_+ + E_y\{J_zJ_x\}_+ + E_z\{J_xJ_y\}_+), \quad (S1)$$

since an ion impurity actually reduces the cubic symmetry ( $T_d \times I$ ) to  $T_d$  (and thus, there is no invariance under inversion) [15]. The ground state splits to two doubly degenerate levels; however, the  $H_E$  does not commute with  $J_z$  for any direction of the field  $\mathbf{E}$ , leading to mixing of the Zeeman states. The latter can be useful to switch on/off the phonon coupling of the alternate qubit,  $\{|-1/2\rangle, |1/2\rangle\}$  (Fig. 1b), provided the splitting  $\delta E_E = 2pE|\mathbf{E}|$  is of the order of that due to stress, e.g., in the GHz range. The transition electric dipole moment,  $p_E$ , can be extracted from experiments: bulk dielectric absorption measurements [22] give  $p_E \simeq 0.26D$ , with  $D = 3.336 \times 10^{-30}$  C m being the Debye unit for e.d.m. (this is supported by single acceptor transport experiments [24]). Thus, a splitting of 1 GHz requires an electric field  $|\mathbf{E}|_{1\text{GHz}} \simeq 3.85 \times 10^5$  V/m, achievable in nanodevices [38]. Note, however, that increasing the field (splitting) exponentially decreases the qubit life time due to acceptor ionization: for  $\delta E = 1$  GHz the life time is  $\tau_{\text{ion}} \approx 12$  s, while for  $\simeq 1.26$  GHz it is  $\tau_{\text{ion}} \approx 12$  ms, etc [38].

These numbers show that there is an experimental “window” for the alternate qubit,  $\{|-1/2\rangle, |1/2\rangle\}$ , introduced in the main text. For example, for a qubit (Zeeman) splitting of  $\delta E_H = 1$  GHz and a strain splitting  $\delta E_e = 1.43$  GHz (ratio of  $r_h \equiv \frac{\delta E_H}{\delta E_e} = 0.7$ ) the coupling factor reaches the maximal value of  $f(r_h, r_e) \simeq 0.4$  for  $\delta E_E = 1$  GHz, i.e.,  $r_e = 0.7$ . Analogously, for a qubit splitting of  $\delta E_H = 2$  GHz this electric field splitting leads to the same coupling factor of 0.4, giving a possibility for a strong acceptor-phonon coupling (Eq. (2) of the main text), and a relatively long (static field) ionization life time.

*Strong coupling of acceptor to confined acoustic phonon.* We account for the acceptor coupling to a quantized phonon

field starting from the Bir-Pikus Hamiltonian, derived for a uniform classical strain field, Eq. (1) (see main text). For low-energy acoustic phonons the interaction Hamiltonian,  $\hat{H}_{\text{ph}}$ , has the same form with the strain operator  $\hat{\epsilon}_{ij}(\mathbf{r}) = \frac{1}{2} \left( \frac{\partial u_i}{\partial r_j} + \frac{\partial u_j}{\partial r_i} \right)$  expressed via the quantized mechanical displacement:  $\mathbf{u}(\mathbf{r}) = \sum_{\mathbf{q}, \sigma} \left( \mathbf{u}_{\mathbf{q}\sigma}(\mathbf{r}) b_{\mathbf{q}\sigma} + \mathbf{u}_{\mathbf{q}\sigma}^*(\mathbf{r}) b_{\mathbf{q}\sigma}^\dagger \right)$ . The mode normalization is  $\int d^3\mathbf{r} \mathbf{u}_{\mathbf{q}\sigma}^*(\mathbf{r}) \mathbf{u}_{\mathbf{q}\sigma}(\mathbf{r}) = \frac{\hbar}{2\rho\omega_{\mathbf{q}\sigma}}$ , so that  $b_{\mathbf{q}\sigma}^\dagger$  creates a phonon in the mode  $(\mathbf{q}, \sigma)$  with energy  $\hbar\omega_{\mathbf{q}\sigma}$  ( $\rho$  is the material mass density) in a mode volume  $\mathcal{V}$ . The vector  $\mathbf{q}$  denotes a collective index of the discrete phonon mode defined via the phonon cavity boundary conditions and mode volume  $\mathcal{V}$ . Similar to cavity QED [33], the phonon-acceptor coupling  $\hbar g_{\mathbf{q}\sigma}^{s's} \equiv \langle s'; \mathbf{q}\sigma | H_{\text{ph}} | s \rangle$  enters in a Jaynes-Cummings Hamiltonian (see, e.g. Ref. [14]):  $H_g \approx \hbar g_{\mathbf{q}\sigma}^{s's} \left( \sigma_{s's}^+ b_{\mathbf{q},\sigma} + \sigma_{s's}^- b_{\mathbf{q},\sigma}^\dagger \right)$ , where we only retain the resonant cavity phonon, and  $\sigma_{s's}^\pm \equiv |s'\rangle \langle s|$  refers to the relevant acceptor transition.

*Phonon-photon translator.* Such a device is based on optomechanical non-linearities that couple in the same bandgap cavity (see Fig. 2e of main text) two photon modes ( $\hat{a}, \hat{a}_p$ ) and a phonon mode  $\hat{b}$ , via optomechanical coupling  $h_{om}$  [31]. For photons in the near-infrared range ( $\lambda_{opt} \approx 1500$  nm) the PPT allows one to couple a quantum optical input/output channel (of frequency  $\omega/2\pi \simeq 200$  THz) to a phonon channel (with  $\omega_d/2\pi \simeq 4 - 8$  GHz), and the coupling between the fields is enhanced by the auxiliary photon pump channel, pumping at the sideband resolved frequency  $\omega_p = \omega - \omega_d - \Delta$  (at pump detuning  $\Delta = 0$  it is at resonance with the red sideband of mode  $\omega$ ). The coherent nature of the photon-to-phonon translator is described by the effective beam-splitter type Hamiltonian [42]:

$$H_{b-s} = -\Delta \hat{b}^\dagger \hat{b} + G_{om} \left( \hat{a}^\dagger \hat{b} + \hat{a} \hat{b}^\dagger \right) \quad (S2)$$

where  $G_{om} \propto h_{om} E_0$  is the enhanced effective coupling, proportional to the pump field amplitude,  $E_0$ . The weak coupling regime,  $G_{om} < \kappa^{opt}$  is needed to avoid total optical reflection, and optimal translation (close to 100%) takes place at a matching condition [31]  $G_{om} = \sqrt{\kappa^{opt} \kappa^{mech}}$  ( $\kappa^{opt}$ ,  $\kappa^{mech}$ , are the couplings of the PPT to respective photon/phonon waveguides).

*Acceptor ionization via optical photons.* Since the photon-to-phonon translator is realized on the same Si nanomembrane (implying a simultaneous photonic/phononic bandgap structure) it is natural to ask how 200 THz photons may affect the qubit lifetime when they reach the acceptor. The corresponding photon energy of 0.82 eV is less than the indirect bandgap in Si ( $\Delta E_{\text{gap}} = 1.1$  eV) and thus interband transitions are not possible. Thus, one considers an “ionization process” of a bound hole going to the continuous spectrum, an analog of the ionization of an (anti)hydrogen atom (the corresponding cross section is thus re-scaled). Correspondingly, one uses the re-scaled values: a free hole mass  $m_A \simeq 0.23 m_e$  in Si, an effective Bohr radius  $a_A^{\text{eff}} = \frac{e^2 Z}{2[4\pi\epsilon_0\epsilon_r]E_A}$ , with the acceptor ionization energy for B:Si,  $E_A \approx 0.044$  eV, and screening factor



$Z \simeq 1.4$ . The total cross section is:

$$\sigma_{\text{phot}} = \frac{32\pi}{3} \frac{\hbar^6}{c\sqrt{2m_A}m_A^3 [a_A^{\text{eff}}]^5 E_f^{2.5} (E_f + E_A)} \frac{1}{[4\pi\epsilon_0\epsilon_r]}, \quad (\text{S3})$$

where  $E_f = \hbar\omega - E_A$  is the final (free) hole energy, and  $c = c_0/\sqrt{\epsilon_r}$  is the speed of light in Si ( $\epsilon_r^{\text{Si}} \simeq 11.9$ ). Since  $E_A \ll E_f$ , the total cross section is suppressed as  $\propto 1/E_f^{3.5}$  (final state energy suppression). Given  $n_c$  photons in cavity volume  $\mathcal{V} \simeq d\lambda^2$  the acceptor life time is  $\tau_{\text{phot}} = 2\mathcal{V}/(n_c c \sigma_{\text{phot}})$  for a maximum photon-acceptor overlap. This limits the ability to perform active photon (sideband) cooling of the phononic cavity (similar to Ref. [10]). However, by placing the acceptor close to a node of the photon cavity, the ionization life time can increase considerably.

---

\* charlie@tahan.com, ruskovr@gmail.com

- [1] H. J. Kimble, *Physica Scripta* **T76**, 127 (1998).
- [2] J. M. Raimond, M. Brune, and S. Haroche, *Rev Mod Phys* **73**, 565 (2001).
- [3] A. Blais *et al.*, *Phys. Rev. A* **69**, 62320 (2004).
- [4] A. A. Houck *et al.*, *Nature* **449**, 328 (2007).
- [5] T. J. Kippenberg and K. J. Vahala, *Science* **321**, 1172 (2008).
- [6] M. Eichenfield *et al.*, *Nature* **462**, 78 (2009).
- [7] S. Weis *et al.*, *Science* **330**, 1520 (2010).
- [8] T. Rocheleau *et al.*, *Nature (London)* **463**, 72 (2010).
- [9] J. D. Teufel *et al.*, *Nature (London)* **475**, 359 (2011).
- [10] J. Chan *et al.*, *Nature* **478**, 89 (2011).
- [11] C. Dong *et al.*, arXiv:1205.2360; J. T. Hill *et al.*, arXiv:1206.0704.
- [12] A. D. O'Connell *et al.*, *Nature* **464**, 697 (2010).
- [13] S. Kolkowitz *et al.*, *Science* **335**, 1603 (2012).
- [14] Ö. O. Soykal, R. Ruskov, and C. Tahan, *Phys. Rev. Lett.* **107**, 235502 (2011).
- [15] G. L. Bir and G. E. Pikus, *Symmetry and Strain-induced Effects in Semiconductors* (Keter Publishing House, Jerusalem, 1974).
- [16] V. N. Smelyanskiy, A. G. Petukhov, and V. V. Osipov, *Phys. Rev. B* **72**, 081304 (2005).
- [17] J. Chan *et al.*, *Appl. Phys. Lett.* **101**, 081115 (2012).
- [18] B. Golding and M. I. Dykman, arXiv, cond-mat/0309147v1.
- [19] See Supplemental Material.
- [20] J. M. Luttinger, *Phys. Rev.* **102**, 1030 (1956).
- [21] H. Neubrand, *Phys. Stat. Solidi (B)* **86**, 269 (1978).
- [22] A. Köpf and K. Lassmann, *Phys. Rev. Lett.* **69**, 1580 (1992).
- [23] Such stress can be created in tensioned membranes [9]. Larger stress ( $\gtrsim 10^7$  Pa) due to a nearby (random) crystal defect [24], or SiGe substrate results in a few hundred GHz splitting.
- [24] L. E. Calvet, R. G. Wheeler, and M. A. Reed, *Phys. Rev. Lett.* **98**, 096805 (2007).
- [25] D. I. Schuster *et al.*, *Nature* **445**, 515 (2007).
- [26] R. Bose *et al.*, *Phys. Rev. Lett.* **108**, 227402 (2012).
- [27] Y. P. Song and B. Golding, *EPL* **95**, 47004 (2011).
- [28] H. Tezuka *et al.*, *Phys. Rev. B* **81**, 161203(R) (2010).
- [29] A. R. Stegner *et al.*, *Appl. Phys. Lett.* **99**, 032101 (2011).
- [30] D. Karaiskaj *et al.*, *Phys. Rev. Lett.* **90**, 016404 (2003).
- [31] A. H. Safavi-Naeini and O. Painter, *New Journal of Physics* **13**, 013017 (2011).
- [32] L. Tian and H. J. Carmichael, *Phys. Rev. B* **46**, R6801 (1992).
- [33] D. F. Walls and G. J. Milburn, *Quantum Optics* (Springer, Berlin 2008, 2008).
- [34] J. M. Fink *et al.*, *Phys. Rev. Lett.* **105**, 163601 (2010).
- [35] M. V. Gustafsson *et al.*, *Nature Physics* **8**, 338 (2012).
- [36] D. Bozyigit *et al.*, *Nature Physics* **7**, 154 (2011).
- [37] M. I. Dykman and M. A. Krivoglaz, *Sov. Phys. Solid State* **29**, 210 (1987).
- [38] G. D. J. Smit *et al.*, *Phys. Rev. B* **70**, 035206 (2004).
- [39] S. Loth *et al.*, *Nature Physics* **6**, 340 (2010).
- [40] P. Rabl *et al.*, *Nature Physics* **6**, 602 (2010).
- [41] J. J. Pla *et al.*, *Nature* **489**, 541 (2012).
- [42] J. Zhang, K. Peng, and S. L. Braunstein, *Phys. Rev. A* **68**, 013808 (2003).